19th Brazilian Congress of Thermal Sciences and Engineering
November 6th–10th, 2022, Bento Gonçalves - RS - Brazil

ENC-2022-0234
MICRO-SCALE MECHANISMS OF PORE BLOCKING BY EMULSION DROPLETS

Clarice de Amorim
Laboratory of Microhydrodynamics and Flow in Porous Media, Department of Mechanical Engineering, Pontifícia Universidade Católica do Rio de Janeiro, Rua Marques de São Vicente, 225, Gávea, Rio de Janeiro, 22451-900 RJ, Brasil
camorim@lmmp.mec.puc-rio.br

Rafael Valladares de Almeida
Repsol Sinopec Brasil, Praia de Botafogo, 300, Botafogo, Rio de Janeiro, 22250-040 RJ, Brasil
rafael.valladares@repsolsinopec.com

Ranena Verónica Ponce Flores
Marcio da Silveira Carvalho
Laboratory of Microhydrodynamics and Flow in Porous Media, Department of Mechanical Engineering, Pontifícia Universidade Católica do Rio de Janeiro, Rua Marques de São Vicente, 225, Gávea, Rio de Janeiro, 22451-900 RJ, Brasil
poncerv@lmmp.mec.puc-rio.br; msc@lmmp.mec.puc-rio.br

Abstract. *Pore-blocking efficiency is a key factor when dilute and stable emulsions are used as flow diversion agents to increase oil recovery and reduce water mobility in preferential flow paths. Emulsion plugging occurs when droplets of the dispersed phase are trapped in the pore throats as they flow through porous media. The capturing phenomenon is highly dependent on the drop-to-pore size ratio, the dispersed phase concentration, and capillary number. Thus, understanding the transport of droplets and the physical mechanisms of pore-blocking at the micro-scale is fundamental for a proper design of emulsion flooding as an enhanced oil recovery (EOR) method. The performance of oil-in-water (O/W) emulsions as pore-blocking agents was investigated by studying the transport of oil droplets through transparent porous media. To this end, a 2D PDMS/glass micromodel with varying constriction sizes was fabricated in-house. Mineral O/W emulsion systems with two distinct drop size distributions were formulated to conduct the tests at different capillary number. The tests were performed by recording the injection pressure response during the sequential flow of an aqueous phase, followed by emulsion (oil drops dispersed in the aqueous phase) and then followed by a second slug of aqueous phase. The association of microfluidic devices and imaging techniques provided a simple way to visualize the droplets' capture phenomena, combining it with the pressure behavior during emulsion flooding. Detailed visualization of the flow was achieved by high-speed live image acquisition at different stages of the test to analyze the features of emulsion flooding and the droplets' capture mechanisms. The results from the flow tests visualization and the pressure drop behavior allowed identifying the capture mechanisms responsible for the droplets' entrapment. Droplets larger than the pore throats were captured by the straining mechanism, while the smaller ones were adsorbed on the pore walls, blocking the pores by droplet accumulation (bridging). At low capillary number (Ca < 1E-4), a larger number of droplets were captured in the pore throats because of the stronger capillary forces. As the capillary number was increased above a threshold value, the viscous force was large enough to overcome the capillary resistance and the droplets were able to deform and re-enter the flow stream. This behavior was quantitatively demonstrated by comparing the mobility of the emulsion to that of the aqueous phase.*
Keywords: *EOR, Emulsion flooding, Oil-in-water emulsion, Injectivity test, Microfluidics*

1. INTRODUCTION

Many conformance control technologies have been introduced to reduce the channeling of water through high permeability channels. In heavy oil reservoirs, the *in-situ* generation of emulsions by alkali-surfactant flooding is known to significantly improve the flooding pattern (Bryan and Kantzas, 2009).
The injection of O/W emulsions has been a promising candidate as a mobility control in capillary-driven displacements in porous media. Emulsion plugging is achieved by trapping droplets of the dispersed phase into pore throats as they

flow through porous media. As the droplets flow through the network constrictions, an extra-pressure drop is needed to overcome the capillary resistance that occurs as the radius of curvature of the drop tip falls into the throat region. This phenomenon is called the Jamin effect (Wright, 1933). For a single droplet, the capillary resistance is given by Laplace's equation, $P_c = 2\sigma cos\theta(1/r_1 - 1/r_2)$, where r_1 and r_2 are the curvature radii of the front part and back end of the droplet as it passes through a constriction. The equation shows that the capillary pressure is not only a function of the droplet size and the pore throat diameter, but also of the oil-water interfacial tension (IFT). Yu *et al.* (2017) reported that emulsion droplets with higher IFT were more efficient in plugging pore throats, as they are less deformable. Ding *et al.* (2020) showed that emulsions with greater IFT gave rise to a sharper increase in pressure at the beginning of injection. At steady state, the pressure drop across the pore throat is not only affected by the capillary resistance, but also by the displacing force caused by the injected fluid and the surface frictional force at the contact area of the emulsion droplet and the pore wall. Several authors have reported a greater permeability reduction at low flow rates (McAuliffe, 1973b; Yu *et al.*, 2017; Chen *et al.*, 2018). At higher flow rates, however, the local pressure drop becomes greater, leading to more droplets overcoming the capillary resistance and deforming to pass through the pore constrictions. The plugging mechanism was also attributed to the frictional resistance occurring both at the pore throat, where the droplets contact the pore wall, and the pore body, where the viscous effect can be approximated using the bulk viscosity (Chen *et al.*, 2018). However, the increase in bulk viscosity alone was reported to contribute very little to the total pressure drop and to the plugging effect (Yu *et al.*, 2018). Instead, the plugging efficiency was found to be primarily from the blocking behavior of emulsion droplets in porous media.

The study of emulsions as a plugging agent to improve oil recovery was first presented by McAuliffe (1973a,b). McAuliffe (1973b) conducted sandstone core flooding tests to study emulsion permeability behavior. He observed that emulsion dramatically reduced water permeability, with the greatest restriction to flow given by emulsions with larger drop sizes. Furthermore, the rate and degree of permeability reduction was shown to be more effective at low pressure gradients. A field test was also implemented for a two-year period, and the results indicated that O/W emulsions effectively increased oil production (McAuliffe, 1973a). McAuliffe (1973b) reported that the droplets decreased water channeling by trapping high-permeability channels, diverting the flow into less permeable zones, and thereby improving fluid distribution. Soo and Radke (1984b) observed that permeability reduction, reported earlier by McAuliffe (1973b), occurred even when the emulsion drop sizes were very much smaller than the size of the pore constrictions. Micromodel observations revealed that permeability reduction mainly arose from retention of drops in the pores. Soo and Radke (1984b) reported that the drops could lodge in pore constrictions (straining capture) or be retained on the surface of sand grains by various physical forces (interception capture). Soo and Radke (1984a) also investigated the effect of velocity on emulsion flow in porous media for a wide range of capillary number. The effect of capillary number and drop-to-pore size ratio on the mobility of O/W emulsions was studied in micro-channel flow and core flooding experiments by Cobos *et al.* (2009) and Romero *et al.* (2011), respectively. Cobos *et al.* (2009) studied the flow of emulsions through a constricted capillary at various flow rates. The results indicated that the flow was dominated by blocking mechanisms caused by drops larger than the capillary diameter. Romero *et al.* (2011) used an experimental setup to determine the effect of capillary number and permeability in emulsion flow through porous media.

Several researchers also described the flow behavior of emulsions in porous media using mathematical models. Alvarado and Marsden (1979) proposed a model based on the effective viscosity, in which the emulsion were treated as a continuous, single-phase fluid. The emulsions were shown to behave as Newtonian fluids at a dispersed phase concentration less than 50%. At higher concentrations, the emulsions behaved like pseudo-plastic fluids. Similar behavior was reported by McAuliffe (1973b), which attributed the non-Newtonian effect to the droplet-to-droplet interaction. Devereux (1974) modified the Buckley-Leverett equation for two-phase flow by including a capillary factor to describe the flow of a stable emulsion in porous media. Although the model properly described the transient behavior of permeability reduction by emulsion injection (McAuliffe, 1973a), it predicted that permeability rises back to its initial value. However, experimental tests showed that permeability does not recover to the initial value after water flooding (Soo and Radke, 1984b). Soo and Radke (1986) developed a simplified filtration model based on deep-bed filtration concepts (Herzig *et al.*, 1970) to quantitatively predict the flow of O/W emulsion in porous media. The model described the interaction between the emulsion droplets and the sand grains and accounted for flow re-distribution and permeability reduction. However, it did not consider drop deformation and re-entrainment within the flow stream. Romero *et al.* (2011) proposed a network model to obtain upscaled Darcy-level response by using pore-level flow description. The model was based on the experimental results reported by Cobos *et al.* (2009). A mobility factor was incorporated to account for the effect of drop deformation on local capillary mobility changes. The network model was able to reproduce qualitatively the experimental data and to describe the dependency of the flow on the local capillary number. However, the model assumed steady state and a constant dispersed-phase concentration throughout the porous medium. In addition, it was based on an idealized circular capillary network. Yu *et al.* (2018) applied the filtration model into capillaries with different diameters and proposed the filtration capillary model, which fully incorporated the geometry of the porous media, emulsion droplet size, emulsion droplet number, and interactions between droplets and porous media. A mathematical model to simulate the plugging pressure drop was recently proposed by Ding and Dong (2019) and improved by Ding *et al.* (2020). Yu *et al.* (2019)

reported that the droplet size was the parameter that mostly affected the emulsion resistance factor, and proposed a mathematical model to describe the flow behavior of emulsions in porous media.
Several works have been conducted to study the use of O/W emulsion as a plugging agent in EOR processes. However, the pore-scale mechanisms are not fully understood, in particular the effect of local flow velocity on the mobility reduction of the aqueous phase. In this work, the relationship between mobility control and capillary number was investigated using a mineral O/W emulsion system with different drop size distributions. The tests were conducted by injecting an aqueous phase, followed by emulsion, and then by a second slug of the aqueous phase, in a microfluidic device with varying constriction sizes. The pressure drop was acquired together with live-images of the droplets flowing through the constrictions during emulsion flooding. The effect of drop-to-pore size ratio on pore plugging was investigated at various capillary number.

2. MATERIALS AND METHODS

2.1 Fluid Properties

The aqueous phase was prepared with the addition of 0.41% w/v sodium dodecyl sulfate (SDS) and 0.0004 wt.% methylene blue in Mili-Q© water (μ_w = 0.8974 cP). The critical micelle concentration (CMC) of SDS was measured and the value (7.01 mM) was lower than that of purified SDS (8.3 mM) reported in literature (Akhlaghi and Riahi, 2019). Therefore, a concentration twice this value was used to ensure the full emulsification of the system. The dispersed phase was composed of 0.1 vol.% Oil-Glo© Ultra Green in Drakeol 7© (μ_o = 15.97 cP). The fluorescent dyes were added to allow for the visualization of both phases separately during the flow tests. The interfacial tension between them was 3.25 mN/m, measured using a Wilhelmy plate (DCAT 25©, Dataphysics Instruments). The phases were fully immiscible over the experimental timescale.

2.2 Emulsion Preparation and Stability

Emulsion Preparation. A stable O/W emulsion was formulated to be used as a pore-blocking agent during the flow test experiments. At first, a diluted system was prepared at a concentration of 5% oleic phase and 95% aqueous phase; however, the stability to creaming was low as the phases began to form two separate layers shortly after emulsification. Therefore, a concentrated system was formulated at an initial concentration of 50% oleic phase and 50% aqueous phase and a total volume of 100 mL. A decantation process was added to the preparation protocol to drain the aqueous phase and obtain a concentrated emulsion. The emulsification process was carried out using an 18-mm rotor-stator dispersing tool (Dispersing Element S25N-18G©, IKA) at 3,000 rpm for 60 seconds. After the homogenization of the phases, the system was put to rest in a separatory funnel for the following 72 hours. The phase separation kinetics was quantified using the Turbiscan© technology. The instrument measures transmission (T) and backscattering (BS) intensities over the sample height, enabling the identification of destabilization mechanisms. Figure 1 illustrates the phase separation of the diluted emulsion over time. After 20 minutes, the phases were clearly separated, with a creamed layer (3.4 mm) of small droplets at the interface. As creaming progressed over time, the aqueous/emulsion interface became well-defined.

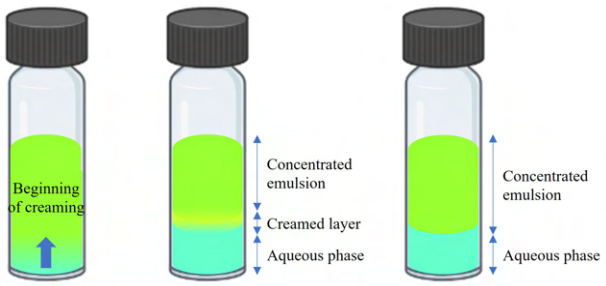

Figure 1: Emulsion destabilization mechanism.

During the decantation process, a total volume of approximately 42 mL of the aqueous phase was drained out. The final volume of the concentrated emulsion was 58 mL, and the new concentration of the system was 85% oleic phase and 15% aqueous phase. A MATLAB© routine developed in-house was used to calculate the number-based drop size distribution of the selected emulsions from microscopic image analysis of their droplets. The stability analysis suggested that the system was stable for the following two weeks after decantation, when it should be used to conduct the flow tests.

Emulsion Stability. In order to evaluate the pore-blocking effect during emulsion injection, two system with small and large drop sizes were proposed. Emulsions with small drop sizes were formulated to have 90% of total drops with a

diameter 30% larger (58.5 μm) than the minimum constriction size (45 μm) of the micromodel, while for emulsions with large drop sizes, the drops were 90% larger (85.5 μm). Stability evaluation consisted in the analysis of the drop size distribution over time and the identification of destabilization mechanisms by Turbiscan Lab©. Combining both results, it was possible to choose the most suitable conditions to prepare the emulsion systems, regarding stability and reproducibility.

2.3 2D Linear PDMS/Glass Micromodel

Micromodel Characterization. A porous media microfluidic device was fabricated in PDMS using standard soft lithography technique (Xia and Whitesides, 1998; McDonald and Whitesides, 2002). The pore network was designed using AutoCAD© and is shown in Fig. 2.

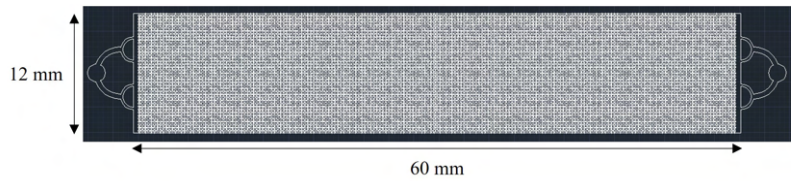

Figure 2: 2D PDMS/glass porous media micromodel design.

The porous medium has a footprint area of 60 x 10 mm^2 and is formed by a repetitive 3 x 3 mm^2 unit cell. Each cell is composed of a 10 x 10 grid of straight and constricted capillaries, randomly distributed. Figure 3 shows the constriction size distribution in each cell. The channels have a square profile with rounded corners of approximately 100 μm depth x 100 μm width, apart from two constriction sizes of 45 μm and 75 μm.

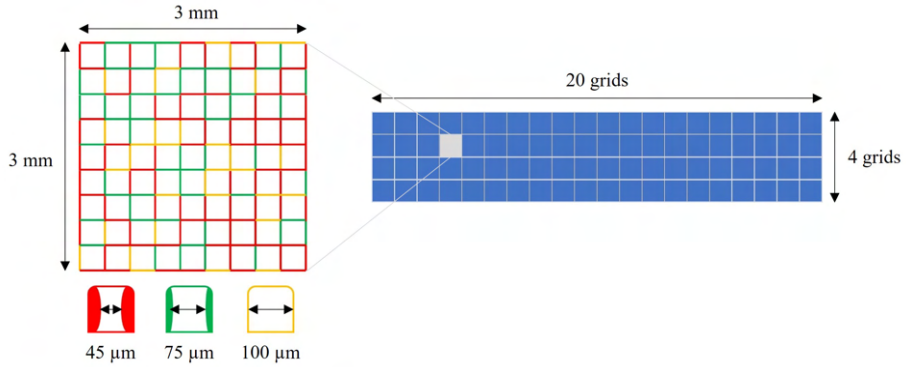

Figure 3: Dimensions of the capillary network.

The pore network is formed by 80 unit cells and 14,400 capillaries, from which 50% represent the 45 μm constriction, 32% the 75 μm constriction, and 28% the straight channel. The porous medium properties were measured experimentally. The network pore volume is 41.30 μL, the porosity, 0.58, and the absolute permeability, 105.30 D. All tests were performed at room temperature.

Surface Wettability. The PDMS surface was treated to render the micromodel a hydrophilic wettability. The hydrophobic property of PDMS (water contact angle > 90°) comes from its basic structure ([-OSi(CH3)2-]n) with many methyl groups (-CH3) and low-surface energy (Thomas *et al.*, 2018). In the last step of microfabrication, the device is submitted to oxygen plasma to bond the PDMS capillary network to the glass. The plasma creates Si-OH polar groupings on the surface of PDMS, changing its properties and making it hydrophilic. The contact angle after plasma treatment goes from 110º to 20º. The hydrophilic behavior is temporary and lasts for 8 hours, beyond which the original surface wettability is gradually restored (Bacharouche *et al.*, 2013).

2.4 Injectivity tests

The performance of O/W emulsions as pore-blocking agents was evaluated through injectivity tests in 2D linear micromodels. The tests were performed by recording the injection pressure response during the sequential flow of aqueous phase, emulsion, and a second slug of aqueous phase. This was done at different capillary number $Ca = \mu v/\sigma$, which is the ratio of viscous to capillary forces. Here, μ, v and σ are respectively the phase viscosity, the interstitial velocity and the phases IFT. The results from the flow test visualization and the pressure drop behavior allowed identifying the capture mechanisms responsible for the droplets entrapment and, therefore, the reduction in the overall permeability.

The interstitial velocities defined to conduct the flow rate experiments ranged from 34.20 to 999.56 ft/d, as shown in Tab. 1. Higher flow rates were expected due to the high permeability ($\sim$ 100 D) of the micromodel. The flow rates were calculated using the cross-section area at the inlet of the pore network.

Table 1: Flow rates used to conduct the injectivity tests.

Interstitial velocity	**Flow rate (Darcy velocity)**			**Capillary number**
ft/day	Total [mL/h]	Concentrated emulsion [μL/min]	Aqueous phase [μL/min]	-
34.20	0.301	0.345	4.682	2.04E-05
99.97	0.881	1.010	13.688	5.96E-05
184.35	1.649	1.890	25.627	1.19E-04
362.49	3.242	3.717	50.393	2.34E-04
508.32	4.546	5.212	70.665	3.28E-04
712.81	6.375	7.308	99.093	4.60E-04
999.56	8.939	10.248	138.956	6.45E-04

Experimental setup. The injection system consisted of two syringe pumps (Syringe Pump 11 Elite©, Harvard Apparatus) coupled to glass syringes (1000 Series GASTIGHT©, Hamilton© Syringe), each one containing the concentrated emulsion (1 mL) and the aqueous phase (2.5 mL), separately. The syringes were connected to a T-valve (Micro-Metering Valve, IDEX), where the phases converged for dilution of the concentrated system in the aqueous phase (Fig. 4). To achieve the final concentration of 5/95 vol.%, the flow rate of each phase was defined, making use of mass balance.

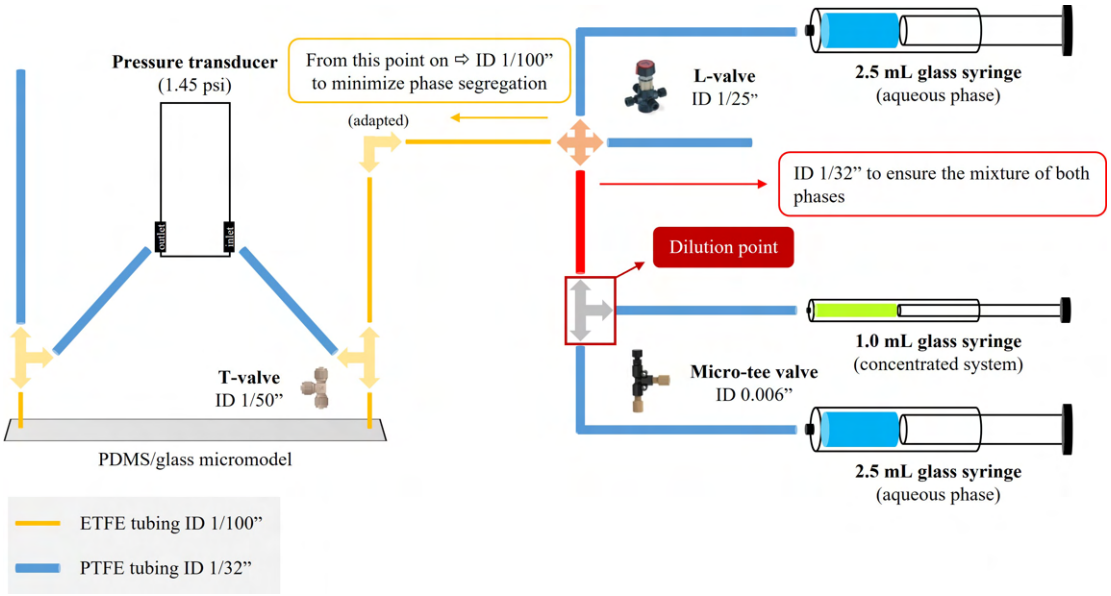

Figure 4: Sketch of the experimental setup.

As sketched in Fig. 4, the connection of the syringes to the L-valve (4-Way Valve, IDEX) was made by a 1/32" ID PTFE tubing (Masterflex© Transfer Tubing PTFE, IDEX). From this point on, a smaller ID tubing (1/100" ID ETFE Tubing, IDEX) was used to minimize the gravitational segregation of the phases. Two micro-tee valves (High-Pressure MicroTee Assembly, IDEX) were coupled to the device to allow the connection of the flow and pressure lines simultaneously to the inlet and outlet ports of the micromodel. A differential pressure transducer (Warmer 0.1 bar) was connected to Labview© to acquire and store the pressure drop. Leica DMi8© Inverted Microscope (Leica Microsystems) was used to visualize the flow during the injectivity tests. The images were acquired using a motorized stage and a high-digital camera (Leica MC170 HD©) coupled to the microscope. Leica Application Suite X© software allowed for image processing and analysis. Detailed visualization of the flow was achieved by high-speed live image acquisition (30 frames per second). Micrographs were taken at different stages of the test to analyze the features of emulsion flooding and the droplets' capture mechanisms. A complete image of the porous medium was acquired by scanning the micromodel in the x- and y-directions and putting all tiles together to form the full image. The acquisition was made with a 2.5x magnification lens, with a resolution of 5 MP (2592 x 1944 pixels).

3. RESULTS

3.1 Emulsion System

The properties of the aqueous and oleic phases, as well as the emulsification conditions of the small and large emulsion systems, are summarized in Tab. 2 and 3, respectively. The aqueous phase viscosity (μ) and the oil-water IFT (σ) were used to calculate the capillary number ($Ca = \mu v/\sigma$) presented in Tab. 1.

Table 2: Properties of the aqueous and oleic phases.

Phase	**Components**	**Density [g/cm^3]**	**Viscosity [cP]**	**IFT [mN/m]**
Aqueous	Mili-Q© water + 0.41% w/v SDS + 0.0004 wt.% MB	0.9975	0.8974	3.25
Oleic	Drakeol 7© + Oil-Glo© Ultra Green (SPI-OGG-16) 0.1 vol.%	0.8432	15.97	

Table 3: Formulation and emulsification conditions of the O/W emulsion systems.

Oleic phase	**Aqueous phase**	**O/W fraction [% v/v]**	**Emulsification conditions**	**d(n,90) [μm]**
Drakeol 7© + OG	Mili-Q© water + SDS + MB	50/50	3000 rpm @ 60 s	$\sim$ 80
			4000 rpm @ 60 s	$\sim$ 60

Figure 5 shows a microscopic image of each system. The image corresponds to a 2 μL drop of diluted emulsion. The scale bar at the right end represents 50 μm. The drop size distributions are shown in Fig. 6 and 7. In both systems, the histogram shows a wide distribution of sizes, characterizing a polydisperse system.

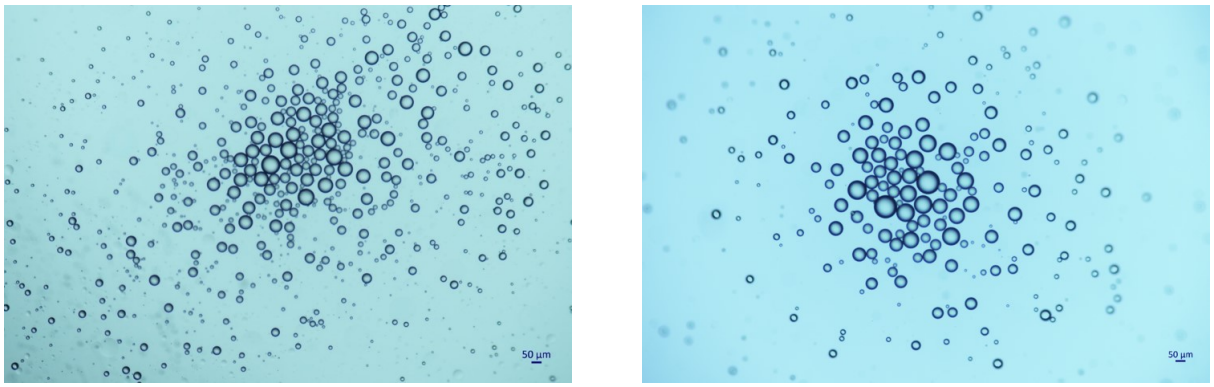

(a) (b)

Figure 5: Emulsions prepared with different emulsification conditions (a) 4,000 rpm for 60 seconds; (b) 3,000 rpm for 60 seconds.

Most of the droplets from the small drop emulsion ranged from 10 to 30 μm (Fig. 6a). The drop size distribution on day 1 shows that 10% of the drops had at least 12.65 μm, 50% at least 24.56 μm, and 90% at least 60.88 μm (Fig. 7a). The emulsion was stable for the following 15 days, without significant changes. The large drop emulsion shows a wider and more uniform distribution of sizes, with drops up to 120 um (Fig. 6b). Most of the drops ranged from 10 to 70 μm and the system was stable for the next 19 days (Fig. 7b).

The drop size distribution of the systems were also analyzed in terms of the constriction size distribution of the microfluidic device and are shown in Fig. 8. The distribution of the small drop system (Fig. 8a) shows that nearly all the drops (99%) were able to flow through both constrictions (45 and 75 μm) without deforming. Knowing that around 80% of the porous network is formed by constricted capillaries, the capture of droplets due to the drop-to-pore size ratio was expected to be low. Figure 8b shows the drop size distribution of the large drop system. In this case, almost half of the drops (46%) were larger than the smallest constriction (45 μm), suggesting the capture of large drops by straining. In addition, 3% of the total drops were larger than the straight channel (100 μm).

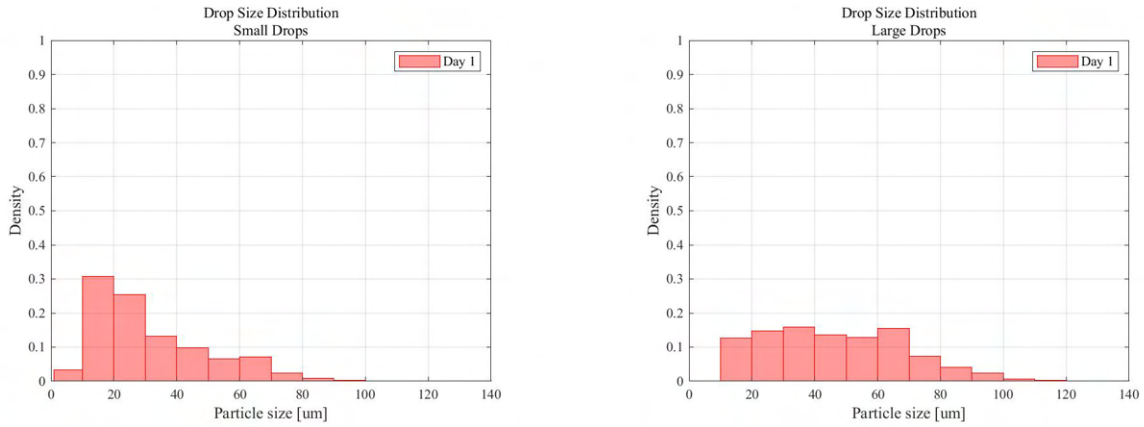

(a) (b)

Figure 6: Drop size distribution of (a) small and (b) large drop emulsion systems.

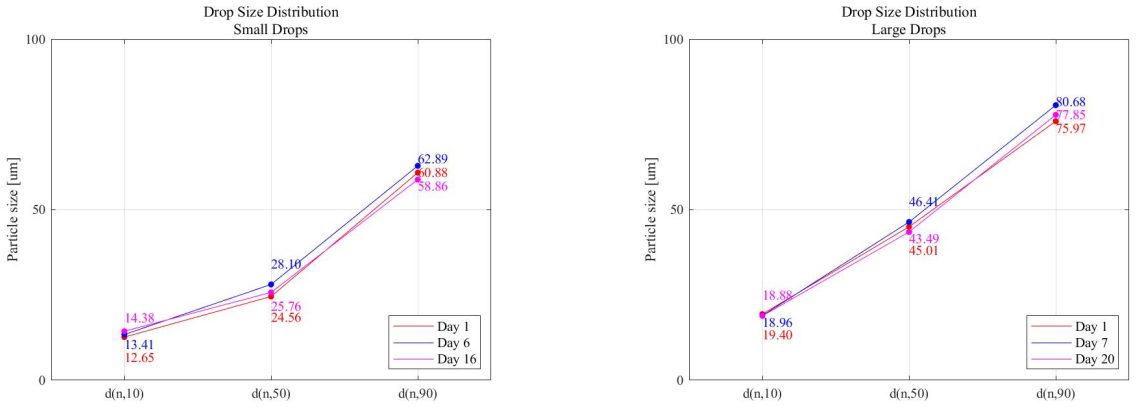

(a) (b)

Figure 7: Stability of (a) small and (b) large drop emulsion systems.

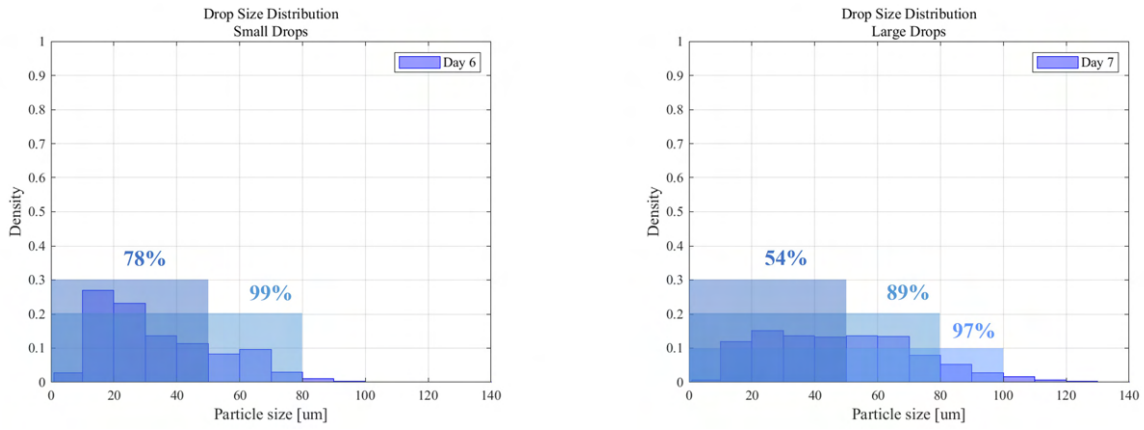

(a) (b)

Figure 8: The drop size distribution of both systems, with (a) small and (b) large drops.

3.2 Injectivity tests

The injectivity tests were conducted using both small and large drop emulsions at different capillary number, presented in Tab. 1. Each test was carried out at a fixed flow rate. Initially, the device was fully saturated with the aqueous phase. After reaching the steady state, the pressure drop was acquired. Following the first water flooding, a total of 17 PV of emulsion were injected. Lastly, a second water flooding was performed, and 14 PV of the aqueous phase were injected.

Mobility Reduction Factor. The mobility reduction factor (f) accounts for the partial pore blocking by emulsion droplets. It was first proposed by Cobos *et al.* (2009) to study the effect of the drop-to-pore size ratio on emulsion flow in porous media. They described f as the pressure difference necessary to drive the flow of the continuous phase to that of the emulsion at the same flow rate:

$$f = \frac{\Delta P_{wf}}{\Delta P_{ef}} \tag{1}$$

Cobos *et al.* (2009) reported that there is a critical capillary number, below which f falls abruptly, and partial blocking occurs. Figure 9 shows f for each test conducted at a fixed flow rate. In the tests performed with the small drop emulsion, the extra-pressure needed for the droplets to flow through the constrictions increased linearly with the capillary number (Fig. 9a). On the other hand, in the tests using the large drop emulsion, the extra-pressure needed to overcome the capillary resistance raised until a critical capillary number (Ca $\approx$ 3E-4), above which the value of f leveled off (Fig. 9b). In both cases, f was observed to vary with the capillary number. This was expected for systems with most part of the drops larger than the pore constrictions (Cobos *et al.*, 2009; Guillen *et al.*, 2012).
In the tests conducted at the lowest flow rate (0.301 mL/h), for the small drop emulsion, f was around 0.15 (Fig. 9a), which means that the mobility of the aqueous phase reduced 85% after emulsion injection. The large drop emulsion, however, showed a lower value of f, around 0.08, indicating a higher reduction in mobility and, consequently, a higher drop capture efficiency (Fig. 9b). The results are in agreement to what was reported earlier by Cobos *et al.* (2009) and Guillen *et al.* (2012) in systems where f is a function of the capillary number. Above a critical value, the viscous pressure is large enough to overcome the capillary resistance to deform the drops ($f \rightarrow 1$); and below this value, f is associated with the extra-pressure drop needed to deform the drops as they flow through the constrictions.

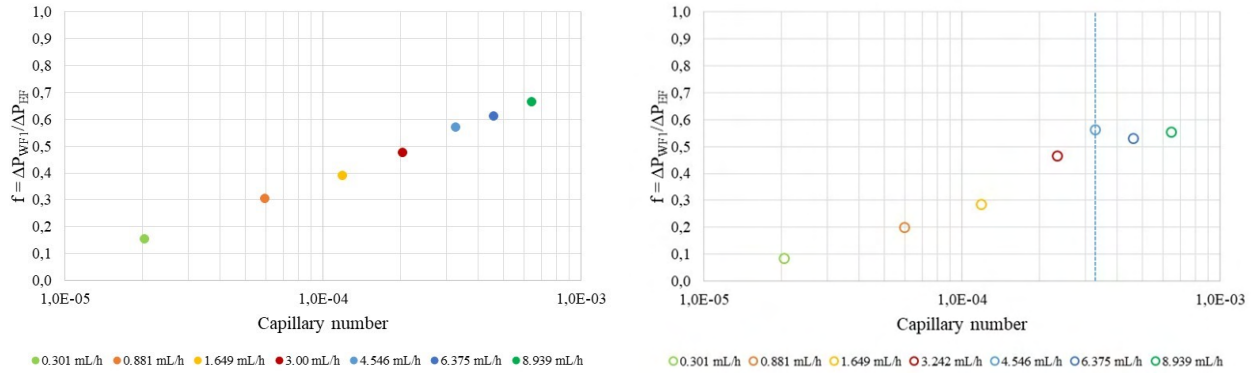

(a) (b)

Figure 9: Mobility reduction factor for (a) small and (b) large drops.

Water Mobility Reduction Factor. A new scaling factor was introduced to quantify the change in water mobility due to the presence of emulsion droplets. As f, it can be written in terms of the average pressure drop:

$$f_w = \frac{\Delta P_{wf1}}{\Delta P_{wf2}} \tag{2}$$

The water mobility reduction factor (f_w), as it was named, compares the mobility of water before and after emulsion flooding, accounting for the effect of the droplets trapped within the porous medium. The value of f_w varies between 0 and 1. In the limiting cases, 0 and 1, f_w is not possible. Experimental tests have shown that irreversible damage is caused by drop retention after emulsion flooding, hence $f < 1$, necessarily. Values near 0 and 1 indicate high- and low-blocking conditions, respectively. For the emulsion with small drop sizes, f_w varied significantly until a critical capillary number (Ca $\approx$ 3E-4), as shown in Figure 10a. The large drop emulsion showed a similar behavior until this critical value, after which f_w leveled out (Fig. 10b).

As shown in Fig. 10, the behavior of f_w was similar to the one observed for f (Fig 9). The comparison between both parameters led to the introduction of the mobility reduction ratio (f_r):

$$f_r = \frac{f}{f_w} = \frac{\Delta P_{wf2}}{\Delta P_{ef}} \tag{3}$$

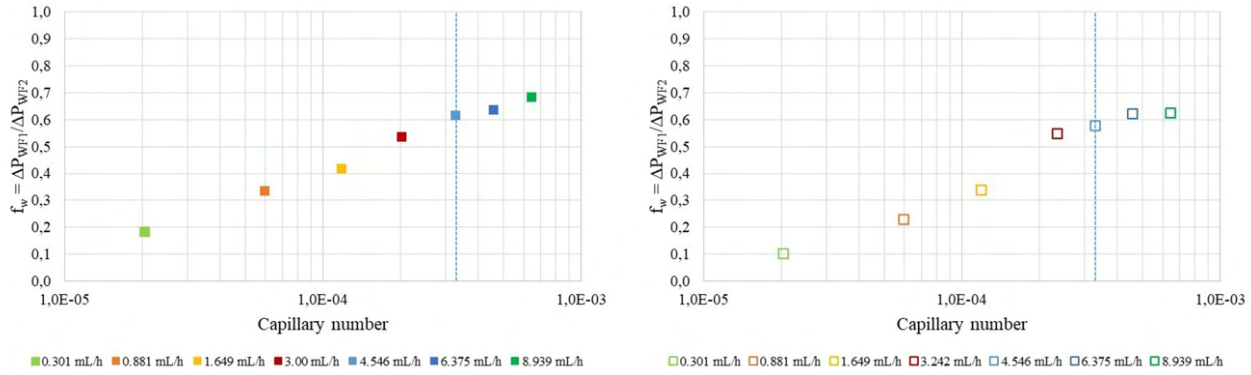

(a) (b)

Figure 10: Water mobility reduction factor for (a) small and (b) large drops.

which accounts for the mobilization of the droplets' during the second water flooding. Figure 11 shows that both systems at the lowest capillary number (0.301 mL/h) exhibit the same value of f_r, around 0.8. For the small drop emulsion, f_r is almost near 1, indicating that a small amount of droplets is mobilized during the second water flooding (Fig. 11a). However, the large drop emulsion showed f_r varying in a lower range, between 0.8 and 0.9, indicating a higher mobilization of droplets (Fig. 11b). Although this behavior is counterintuitive, it was demonstrated experimentally by Ng *et al.* (1978), while studying ganglia mobilization in porous medium (Melrose, 1974). Ng *et al.* (1978) showed that the critical capillary number to mobilize an individual ganglion is inversely proportional to its length in the flow direction.

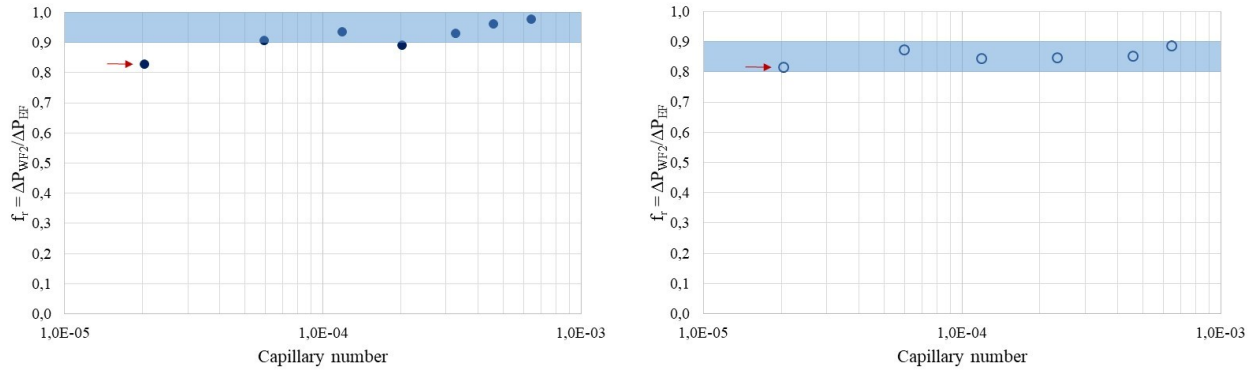

(a) (b)

Figure 11: Mobility reduction ratio for (a) small and (b) large drops.

The water mobility reduction factor also represents the reduction in permeability caused by drop retention. It can be applied as an upscaling factor to account for the reduction in the absolute permeability after emulsion flooding. Therefore, the viscous pressure drop required to displace the aqueous phase over a length L, after emulsion injection, can be described by Darcy's law in terms of f_w:

$$\Delta P_v = \frac{1}{f_w}\frac{\mu_w}{K}\frac{Q}{A}L \tag{4}$$

The permeability damage can be estimated by comparing the absolute permeability to the continuous phase before and after emulsion injection, as shown in Fig. 12. It can be written as:

$$k_D = \frac{k_{after}}{k_{before}} \tag{5}$$

where $k_{before} = k_{after}/f_w$. Here, k_{before} and k_{after} are the absolute permeability values before and after emulsion injection, respectively. The reduction in permeability caused by the small drop emulsion is observed to vary linearly with the capillary number (Fig. 12a), similar behavior shown by f. The large drop emulsion, on the other hand, shows a significant reduction until Ca $\approx$ 2E-4, beyond which the damage caused due to the presence of the droplets seems to level out (Fig. 12b).

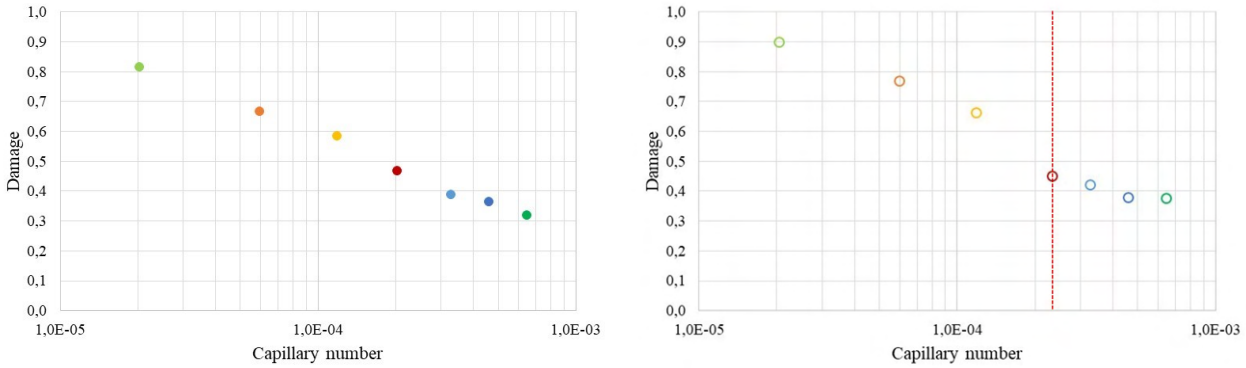

(a) (b)

Figure 12: Permeability damage caused by pore blocking by (a) small and (b) large drops.

Figure 13 shows a full image of the micromodel after the second water flooding for tests at two different capillary number, 2.04E-5 and 5.96E-5, respectively. The test conducted at low capillary number (Ca = 2.04E-5) exhibited a permeability damage 17% higher than that at higher capillary number (Ca = 5.96E-5). At the low capillary number, Figure 13a shows a single flow path created by the aqueous phase at the lower part of the device. When the capillary number was increased, several fingers were created throughout the porous medium (Fig. 13b). The aqueous phase was able to mobilize a significant number of droplets, diverting the flow throughout the micromodel.

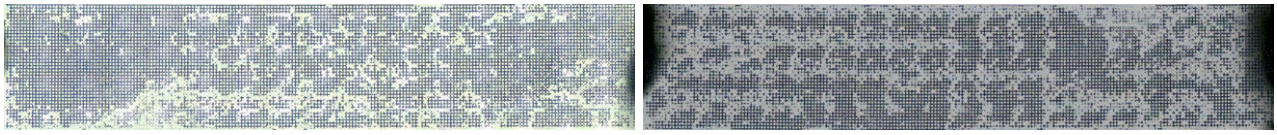

(a) (b)

Figure 13: A full image of the micromodel after the second water flooding at (a) low (Ca = 2.04E-05) and (b) high capillary number (Ca = 5.96E-05).

Pore-blocking mechanisms. The experimental study of Soo and Radke (1984b) showed that emulsion droplets are captured by straining and/or interception while flowing through porous media. To better understand these mechanisms, photo-micrographs were taken at different steps during emulsion flooding. Straining was the dominant capture mechanism at high capillary number (Ca > 1E-4), in agreement with previous results reported by Soo and Radke (1986).
Figure 14 shows a large drop initially captured by straining. The droplet was lodged in a pore body smaller than its size (Fig. 14a). An increase in the local pressure drop mobilized the droplet toward the constriction. As the pressure built up, the droplet was able to deform and pass through the pore throat (Fig. 14b), entering a subsequent pore body (Fig. 14c). No droplet break-up was observed during this event.

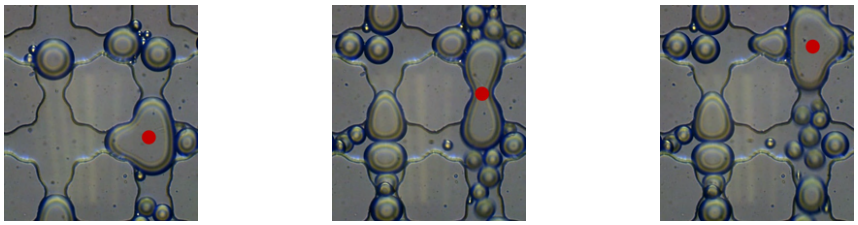

(a) (b) (c)

Figure 14: A large droplet (marked in red) initially captured by straining.

The accumulation of droplets at the pore wall was observed to reduce the effective pore throat width, favoring the straining of other droplets and increasing the local flow resistance. Figure 15 shows a simple sequence of small droplets captured by interception restraining the pore entrance.
Drops adhered to the pore walls and/or trapped in recirculation eddies were observed at low capillary number. Soo and Radke (1984a) reported that velocity effects are important when the capture of small droplets is in the secondary-minimum energy well and the velocity is close to a critical re-entrainment value.

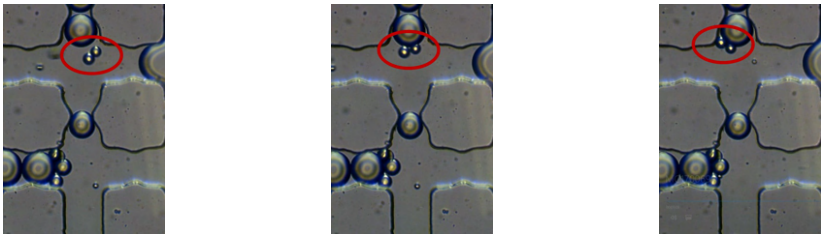

(a) (b) (c)

Figure 15: A sequence of small drops (circled in red) being captured by interception.

4. CONCLUSIONS

The local mobility reduction of the flow by the presence of trapped droplets was investigated at different capillary number. The pressure drop response at each flow rate was acquired simultaneously with live-images of the flow during emulsion flooding. The effect of the drop-to-pore size ratio was analyzed in terms of the drops' capture efficiency. Systems with large drops showed a higher capture efficiency and, consequently, a higher permeability damage after emulsion flooding. Although larger drops demonstrated high blocking efficiency, the results showed that small droplets exhibited higher resistance to mobilization. The accumulation of small droplets increased the local flow resistance, reducing the fluid velocities near saturated regions. In the other hand, large drops captured by straining showed less resistance to mobilization at high capillary number. The drops were able to deform and re-entrain the flow when the viscous pressure was higher than a threshold value, imposed by capillary forces. This behavior was quantitatively demonstrated by the scaling factors f and f_w, and is in agreement with earlier studies.

5. ACKNOWLEDGEMENTS

This work was carried out as part of the project entitled "Emulsion Injection as a Flow Diversion Method to Increase Oil Recovery and Reduce Water Production" funded by Repsol Sinopec Brazil. The authors acknowledge the financial support from Repsol Sinopec Brazil and the Coordination of Superior Level Staff Improvement (CAPES).

6. REFERENCES

Akhlaghi, N. and Riahi, S., 2019. "Salinity effect on the surfactant critical micelle concentration through surface tension measurement". *Iranian Journal of Oil and Gas Science and Technology*, Vol. 8, No. 4, pp. 50–63.

Alvarado, D. and Marsden, S., 1979. "Flow of oil-in-water emulsions through tubes and porous media". *Society of Petroleum Engineers Journal*, Vol. 19, No. 06, pp. 369–377.

Bacharouche, J., Haidara, H., Kunemann, P., Vallat, M.F. and Roucoules, V., 2013. "Singularities in hydrophobic recovery of plasma treated polydimethylsiloxane surfaces under non-contaminant atmosphere". *Sensors and Actuators A: Physical*, Vol. 197, pp. 25–29.

Bryan, J. and Kantzas, A., 2009. "Potential for alkali-surfactant flooding in heavy oil reservoirs through oil-in-water emulsification". *Journal of Canadian Petroleum Technology*, Vol. 48, No. 02, pp. 37–46.

Chen, Z., Dong, M., Husein, M. and Bryant, S., 2018. "Effects of oil viscosity on the plugging performance of oil-in-water emulsion in porous media". *Industrial & Engineering Chemistry Research*, Vol. 57, No. 21, pp. 7301–7309.

Cobos, S., Carvalho, M. and Alvarado, V., 2009. "Flow of oil–water emulsions through a constricted capillary". *International Journal of Multiphase Flow*, Vol. 35, No. 6, pp. 507–515.

Devereux, O.F., 1974. "Emulsion flow in porous solids: I. a flow model". *The Chemical Engineering Journal*, Vol. 7, No. 2, pp. 121–128.

Ding, B. and Dong, M., 2019. "Optimization of plugging high mobility zones in oil sands by injection of oil-in-water emulsion: Experimental and modeling study". *Fuel*, Vol. 257, p. 116024.

Ding, B., Dong, M. and Yu, L., 2020. "A model of emulsion plugging ability in sandpacks: Yield pressure drop and consistency parameter". *Chemical Engineering Science*, Vol. 211, p. 115248.

Guillen, V.R., Romero, M.I., da Silveira Carvalho, M. and Alvarado, V., 2012. "Capillary-driven mobility control in macro emulsion flow in porous media". *International Journal of multiphase flow*, Vol. 43, pp. 62–65.

Herzig, J., Leclerc, D. and Goff, P.L., 1970. "Flow of suspensions through porous media—application to deep filtration". *Industrial & Engineering Chemistry*, Vol. 62, No. 5, pp. 8–35.

McAuliffe, C.D., 1973a. "Crude-oil-water emulsions to improve fluid flow in an oil reservoir". *Journal of Petroleum Technology*, Vol. 25, No. 06, pp. 721–726.

McAuliffe, C.D., 1973b. "Oil-in-water emulsions and their flow properties in porous media". *Journal of petroleum technology*, Vol. 25, No. 06, pp. 727–733.

McDonald, J.C. and Whitesides, G.M., 2002. "Poly (dimethylsiloxane) as a material for fabricating microfluidic devices". *Accounts of chemical research*, Vol. 35, No. 7, pp. 491–499.

Melrose, J., 1974. "Role of capillary forces in detennining microscopic displacement efficiency for oil recovery by waterflooding". *Journal of Canadian Petroleum Technology*, Vol. 13, No. 04.

Ng, K., Davis, H. and Scriven, L., 1978. "Visualization of blob mechanics in flow through porous media". *Chemical Engineering Science*, Vol. 33, No. 8, pp. 1009–1017.

Romero, M.I., Carvalho, M.S. and Alvarado, V., 2011. "Experiments and network model of flow of oil-water emulsion in porous media". *Physical Review E*, Vol. 84, No. 4, p. 046305.

Soo, H. and Radke, C., 1984a. "Velocity effects in emulsion flow through porous media". *Journal of Colloid and Interface Science*, Vol. 102, No. 2, pp. 462–476.

Soo, H. and Radke, C., 1986. "A filtration model for the flow of dilute, stable emulsions in porous media—i. theory". *Chemical Engineering Science*, Vol. 41, No. 2, pp. 263–272.

Soo, H. and Radke, C.J., 1984b. "Flow mechanism of dilute, stable emulsions in porous media". *Industrial & engineering chemistry fundamentals*, Vol. 23, No. 3, pp. 342–347.

Thomas, S., Mozetic, M., Cvelbar, U., Spatenka, P. and Praveen, K.M., 2018. *Non-thermal Plasma Technology for Polymeric Materials: Applications in Composites, Nanostructured Materials, and Biomedical Fields*. Elsevier.

Wright, R., 1933. "Jamin effect in oil production". *AAPG Bulletin*, Vol. 17, No. 12, pp. 1521–1526.

Xia, Y. and Whitesides, G.M., 1998. "Soft lithography". *Angewandte Chemie International Edition*, Vol. 37, No. 5, pp. 550–575.

Yu, L., Ding, B., Dong, M. and Jiang, Q., 2018. "Plugging ability of oil-in-water emulsions in porous media: experimental and modeling study". *Industrial & Engineering Chemistry Research*, Vol. 57, No. 43, pp. 14795–14808.

Yu, L., Ding, B., Dong, M. and Jiang, Q., 2019. "A new model of emulsion flow in porous media for conformance control". *Fuel*, Vol. 241, pp. 53–64.

Yu, L., Sang, Q., Dong, M. and Yuan, Y., 2017. "Effects of interfacial tension and droplet size on the plugging performance of oil-in-water emulsions in porous media". *Industrial & Engineering Chemistry Research*, Vol. 56, No. 32, pp. 9237–9246.

7. RESPONSIBILITY NOTICE

The authors are solely responsible for the printed material included in this paper.